

A very low temperature STM for the local spectroscopy of mesoscopic structures

N. Moussy, H. Courtois and B. Pannetier

Centre de Recherches sur les Très Basses Températures-C.N.R.S. associated to Université Joseph Fourier,
25 Ave. des Martyrs, 38042 Grenoble, France

(October 30, 2018)

We present the design and operation of a very-low temperature Scanning Tunneling Microscope (STM) working at 60 mK in a dilution refrigerator. The STM features both atomic resolution and micron-sized scanning range at low temperature. We achieved an efficient thermalization of the sample while maintaining a clean surface for STM imaging. Our spectroscopic data show unprecedented energy resolution. We present current-voltage characteristics and the deduced local density of states of hybrid Superconductor-Normal metal systems. This work is the first experimental realization of a local spectroscopy of mesoscopic structures at very low temperature.

I. INTRODUCTION

Mesoscopic effects in metallic structures are quantum interference phenomena based on electron phase coherence.¹ This coherence persists over a length L_φ which increases with decreasing temperature and usually reaches about $1\ \mu\text{m}$ in clean metals below 1 K . In particular, much interest was recently devoted to the proximity effect occurring in hybrid mesoscopic structures made of a Superconductor (S) in clean contact with a Normal metal (N).² So far, transport measurements have been the primary means of investigation of such mesoscopic structures. A promising alternative approach is the use of a very-low temperature scanning probe. For instance, a Scanning Tunneling Microscope (STM) enables one to access the local density of states with atomic spatial resolution. With regards to the proximity effect, the local modification of the density of states has been measured at moderately low temperature ($T > 1\text{ K}$) by several groups in various kinds of samples.³⁻⁶

Here, we present the design and operation of a very-low temperature STM operating at 60 mK in a dilution refrigerator and featuring a large ($\approx 6\ \mu\text{m}$) scan range. Operating at such very low temperatures allows one to gain access to a wide range of phenomena and reduces the thermal smearing of the measured density of states. The combination of very-low temperature techniques with the constraints of scanning probe microscopy is indeed a demanding task. This explains the relatively small number of such studies. To our knowledge, the only spectroscopic measurement at a temperature below 100 mK was reported in NbSe_2 .⁷ A very-low temperature Atomic Force Microscope was operated at 30 mK in a 9 T magnetic

field.⁸ Images of adsorbed He atoms were obtained at 90 mK .⁹ Various STMs operating at 300 mK have also been recently reported.¹⁰

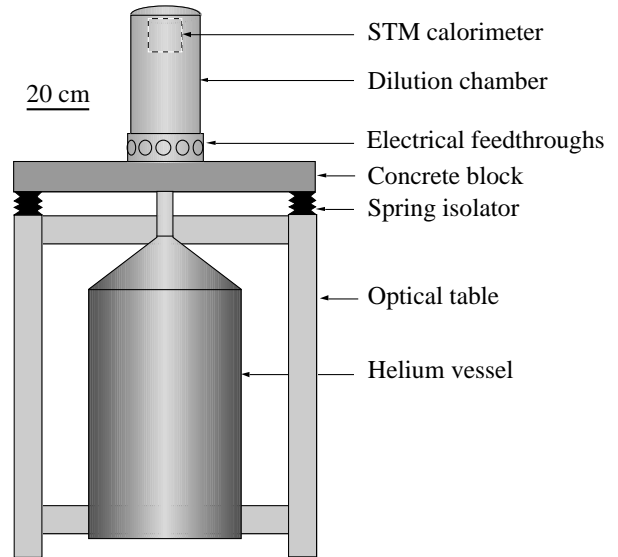


FIG. 1. Schematics of the cryostat. The cryostat is fixed on a concrete block supported by an optical table with 4 spring isolators. The pressurized He vessel underneath provides the ^4He flow. The pumps are located in a nearby acoustically isolated room.

II. CRYOGENICS

We use a home-made upside-down dilution refrigerator called "sionludi" with the cold plate placed upwards.¹¹ Figure 1 shows a schematic of the whole setup. The cryostat is isolated from the building vibrations by spring isolators with a 2 Hz resonant frequency. The connection to the pumps of the dilution circuit is made of flexible pipes and tubes passing through heavy concrete blocks. The base temperature with the measurement wiring installed is about 60 mK in a cylindrical volume of diameter 13 cm and height 13 cm .

The main advantages of our cryostat are its natural rigidity, the handy horizontal access and a very rapid cooling/heating cycling. The whole cryostat is enclosed in a single vacuum which is sealed with a room-temperature o-ring. There is no N_2 bath and therefore no N_2 boiling vibrations. The 4 K stage is cooled by a ^4He flow from a pressurized helium vessel. During cool-

ing down to 4 K , a large flow of ${}^3\text{He} - {}^4\text{He}$ mixture thermalizes the dilution stage. Depending on the ${}^4\text{He}$ flow, the cooling down to 4 K lasts about 6 hours. The ${}^3\text{He} - {}^4\text{He}$ mixture is injected in the cryostat at a pressure between 0.5 and 2 bar . After reaching 4 K , a fast cooling down to 1.5 K of the dilution stage is ensured by a Joule-Thomson expansion of the mixture through a dedicated circuit. In the dilution regime, the limit temperature is reached within 4 hours with the STM installed. The cooling power is about $10\ \mu\text{W}$ at 100 mK .

The STM is enclosed in a hermetic calorimeter screwed on the mixing chamber. This calorimeter is sealed with an In seal inside a glove box. The controlled $\text{N}_2 - \text{He}$ dry atmosphere enables us to minimize surface contamination. Before cooling, the calorimeter is rinsed several times with pure He gas while heating the sample for outgassing. The calorimeter is then closed with the help of a stainless steel valve with a He pressure of about 10^{-2} mbar . At low temperature ($T < 20\text{ K}$), active carbon grains pump the residual He atmosphere.

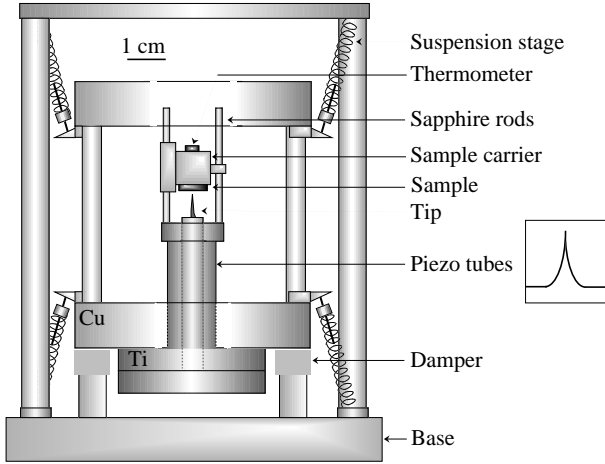


FIG. 2. Design of the STM head. The two concentric piezo-electric tubes are glued with Stycast on Ti parts fixed on the Cu body of the STM. The whole STM head is suspended by six springs. The sample carrier slides on the two sapphire rods of the outer piezo-electric tube. It also includes a special temperature control (see text). The coarse approach pulse waveform is schematically shown.

III. THE STM

A. The STM head

The STM head is very rigid, 500 g in weight and suspended with six springs. The resonant frequency of this isolation stage has been adjusted to 10 Hz in order to avoid any resonance with the cryostat isolation stage. The tip is placed near both the inertial center of the suspended head and the symmetry center of the spring's fixation points. This reduces the displacement of the tip with respect to the base. Residual oscillations of the head

are damped by sliding friction.

The head is made of two concentric 2.5 cm long piezo-electric PZT-5A tubes. The piezo tubes are glued with Stycast to Ti parts. Differential expansion stress during thermal cycles are then minimized since Ti and Stycast thermal expansion coefficients are close to that of PZT.¹² The inner tube holds the tip : it is a XY scanner with a $6 \times 6\ \mu\text{m}^2$ scan range at low temperature for a $\pm 220\text{ V}$ voltage sweep. Its inner electrode is used for the withdrawal of the tip during lateral displacements or coarse approach steps. The outer piezoelectric tube serves to regulate the sample-tip distance regulation and ensures the inertial displacement. It holds the two sapphire rods on which the sample inertial carrier slides.

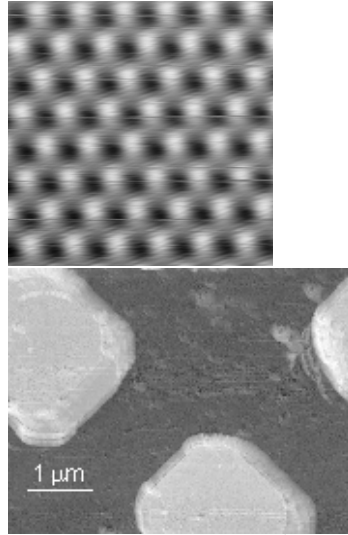


FIG. 3. Left : $15 \times 15\text{ \AA}^2$ STM image of the atomic lattice of 2.4 \AA periodicity at a HOPG (graphite) surface. Right : $5.7 \times 4.3\ \mu\text{m}^2$ STM image of a mesoscopic sample made of a square array of 300 \AA -thick Nb square islands with a Au layer deposited on top of it. The lattice parameter is $4\ \mu\text{m}$. Both images are unfiltered and have been taken at a sample temperature of 60 mK with the same piezo-electric tubes.

B. The sample coarse approach

Our vertical inertial motor is directly inspired from the work of C. Renner et al.¹³ The carrier is made of two brass parts clamped on the sapphire rods by a compressed spring. The sliding friction force is about 40 g while the carrier weight is 12 g . Each part has three well-defined contact points on the rods. The pulse waveform is a double parabola, so that the acceleration is constant except at the crossover point (see Fig. 2 inset). The duration of one pulse is about $240\ \mu\text{s}$. A single pulse makes the carrier move 50 to 1400 nm at ambient temperature and 10 to 200 nm at $T < 4\text{ K}$. Both upwards and downwards displacement are possible.

We found that the step length remain reliable as long as the sapphire tubes remain free of adsorbed water. Dur-

ing cooling, the carrier is therefore kept at a temperature about $40 K$ larger than the cryostat temperature. This is ensured by a strain gauge used as a heater and a Pt thermometer, both glued on the carrier. This procedure ensures a low cryosorption on the sapphire rods and on the sample surface. The heating is stopped at a cryostat temperature of $60 K$.

An automatic coarse approach is performed during cooling from $T = 60 K$ to $4 K$. As the sample is placed about 1 mm above the tip at ambient temperature, about 4000 steps are necessary to reach the tunnel contact. One step consists in withdrawing the tip with the inner tube, sending a pulse on the outer tube and slowly approaching the tip within 5 seconds. When a tunnel current is detected, the approach is stopped and the tip is withdrawn to a rest position. Usually no thermal drift is observed below $20 K$.

C. Thermalization

The experimental challenge here is to ensure both an efficient thermalization and a good mechanical decoupling to vibrations for the microscope. Thermalization below $1 K$ is ensured through copper braids connecting the base, the suspended head and the Ti parts glued on top of the two tubes. The sample carrier and the tip are also thermalized through their attached Cu measurement wires. A carbon resistor glued on the sample carrier is used for the measurement of the sample temperature below $1 K$.

We have characterized the amount of heating due to both coarse approach and scanning. Starting from the STM base temperature (60 mK), the sample temperature after a single coarse approach step reaches instantly about 100 mK . It afterwards drops down to 60 mK in a few minutes. A continuous displacement with about ten steps by second heats the sample up to about $1 K$ and the mixing chamber to 350 mK . This corresponds to an injected power of about $250 \mu\text{W}$ and a dissipated energy of about $25 \mu\text{J}$ per step. Image scanning also heats the system but can be minimized significantly at low scanning speed. For example, large field imaging ($6 \times 6 \mu\text{m}^2$) on a large corrugation of the order of 300 \AA may heat the sample to about 100 mK when the scanning speed is about 500 nm/s .

D. The STM electronics

Our electronics are home-made. Each incoming wires is filtered by radio-frequency filters at the cryostat entrance. Switchable very low frequency filters with a 0.5 Hz cut-off are placed at the high-voltage amplifiers outputs. They are switched on during spectroscopies in order to increase stability of the tip-sample distance. The tip bias undergoes a $\frac{1}{10}$ reduction at 60 mK so that the

effect of extrinsic noise is reduced. The tunnel current preamplifier features a 12 kHz bandwidth. It works at room temperature but the $100 \text{ M}\Omega$ feedback resistance of the input op-amp is thermalized at $4.2 K$. This reduces the contribution of its thermal noise to the total current noise. The measured total noise is $4.5 \text{ fA}/\sqrt{\text{Hz}}$ below 300 Hz including the current noise from the op-amp of about $1.5 \text{ fA}/\sqrt{\text{Hz}}$. Above 300 Hz , the noise increases linearly with the frequency because the op-amp voltage noise biases the capacitance of the coaxial wire.

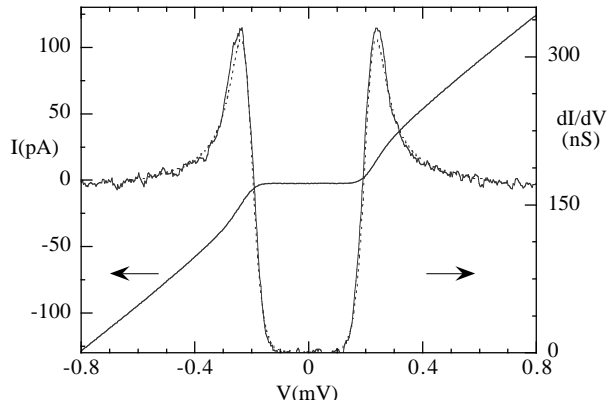


FIG. 4. I-V characteristics and its numerical derivative (= differential conductance) measured by STM on a superconducting layer of Al at 60 mK . The I-V characteristic is an average over 20 curves. The dashed line is a fit using a BCS density of states convoluted with a thermal Fermi distribution. The fit parameters are the values of the superconducting gap $\Delta_{\text{Al}} = 210 \mu\text{eV}$ and an effective temperature $T_{\text{eff}} = 210 \text{ mK}$.

IV. FIRST RESULTS

A. Images

Mesoscopic samples prepared by standard lithography often exhibit large corrugation of several hundreds of \AA . With such a large relief, we need sharp tips with a large aspect ratio. We use electrochemically-etched Pt/Ir tips because of their stiffness and low natural oxidation. Tips are prepared with the technique described by Lindahl et al.,¹⁴ with the difference that we avoid bending the tip but instead immerse it in the liquid with a large angle. With this method, we obtain routinely a tip radius of about 30 nm .

Figure 3 shows two images taken at the temperature of 60 mK . Let us point out that the ratio of the image sizes is larger than 1000. We achieved atomic resolution on HOPG graphite at both room temperature and very low temperature (60 mK). On mesoscopic samples, imaging on the scale of a few microns is performed very slowly in order to avoid tip crash and heating of the sample. A typical 128×128 pixel image of $5 \times 5 \mu\text{m}^2$ is acquired in about half an hour. These images show that we are able to keep a clean sample surface, i.e., without noticeable

contamination, during cooling. Heating the sample during cooling was found to be necessary in order to obtain such a surface quality.

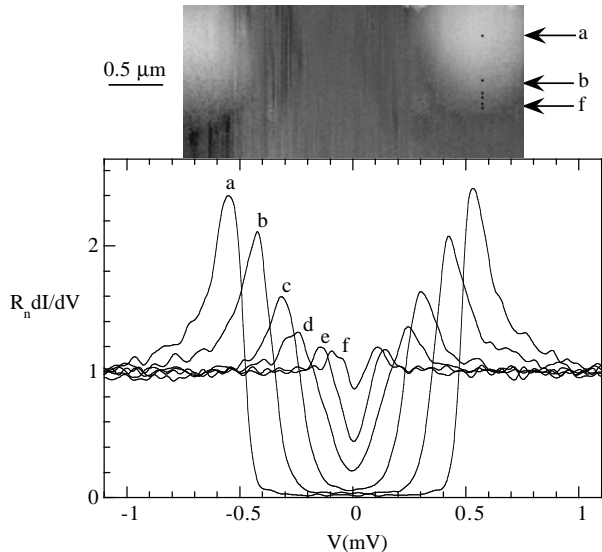


FIG. 5. Top : $5 \times 2.2 \mu\text{m}^2$ STM image at 70 mK of sample made of Nb islands covered by a uniform 200 \AA Au layer. The locations where the tunnel spectra were measured are indicated by a black pixel. Bottom : Measured differential conductance at various locations on the sample. At the center of the Nb island, the Nb is 440 \AA thick and the gap is the largest. The tunnel conductance was about 300 nS .

B. Density of states measurements

In order to measure a local density of states, we acquire I-V characteristics of a fixed sample-tip tunnel junction. The tip feedback is first set to a large response time constant, the high-voltage low-pass filters are switched on and the feedback loop is opened. The bias voltage is then swept while the tunnel current is measured. This sweep lasts up to 20 s without modification of the junction. We usually average over 10 to 40 I-V curves in order to reduce the noise. The experimental I-V characteristic is then numerically differentiated in order to obtain the differential conductance $dI/dV(V)$. The differential conductance coincides with the local density of states in the zero-temperature limit.

As a test experiment, we measured the density of states at the surface of plain superconducting layers. Figure 4 shows the experimental I-V characteristic and the deduced differential conductance dI/dV at the surface of an Al layer. These data are representative of the quality of our spectroscopy measurements, although in this case the tip is presumably dug into the surface Al oxide. From our measurements, we can estimate a maximum vibration amplitude of about 10^{-2} \AA . The differential conductance dI/dV clearly shows a superconducting gap. It is zero in the vicinity of the Fermi level ($eV = 0$). We described this data using a BCS density of states

convoluted by a thermal distribution function, without broadening by a finite quasiparticle lifetime.¹⁵ The value of the Al gap $\Delta_{\text{Al}} = 210 \mu\text{eV}$ derived from the fit is in agreement with the expected value. The effective temperature derived from the fit is $T_{\text{eff}} = 210 \text{ mK}$. As the sample temperature was in every case about 60 mK , the origin of this effective temperature increase is unclear at present. Nevertheless, our data show that we can identify the measured differential conductance with the local density of states if the desired resolution remains larger than $2k_B T_{\text{eff}} = 36 \mu\text{eV}$.

Figure 5 shows a preliminary experiment performed on a Normal metal-Superconductor junction. We fabricated the sample by successive in-situ evaporation of Nb and Au in a UHV chamber. Nb was evaporated first through a Si mask put in contact with the Si substrate. The mask was a $5 \mu\text{m}$ thick Si membrane patterned by e-beam lithography. The mask was then mechanically removed and a uniform Au layer was deposited, without breaking vacuum. This ensures a high transparency of the Nb-Au interface. The Nb islands are about $1.8 \mu\text{m}$ wide and their center to center distance is $4.3 \mu\text{m}$. Only a few Nb islands are accessible within the STM scan range. As shown in the STM image, the Nb islands are rather rounded. This is due to the thickness of the mask and the imperfection of the contact between the mask and the substrate.

We measured the differential conductance at various locations while moving the tip away from the center of a Nb island. In order to reduce the hysteresis of the scanner below 10 nm , we had to use a scanning speed below 10 nm/s . In Fig. 5, we clearly see the spatial dependence of the density of states. The spectrum with the largest gap was taken near the center of the Nb island : it can be well described by a BCS density of states. The magnitude of the energy gap is reduced compared to the Nb value because of the influence of the Au layer. Away from the Nb island, the density of states has a triangular shape. It is the signature of the proximity effect. The characteristic decay length of the proximity effect appears to be about 120 nm . A detailed description of our results by the quasiclassical theory¹⁶ is under way.

This work greatly benefited from the help of A. Benoit, H. Rodenas and K. Hasselbach in the design, fabrication and optimization of the "sionludi" cryostat. We thank the CRTBT technical staff for their various contributions to the design and construction of the STM setup. We thank W. Belzig, A. Bezryadin, I. Maggio-Aprile, C. Renner, D. Rodichev, H. Takayanagi and Y. de Wilde for discussions. We acknowledge discussions within the "Dynamics of superconducting nanocircuits" TMR network and support from DRET and Région Rhône-Alpes.

- ¹ Y. Imry, *Introduction to Mesoscopic Physics*, Oxford University Press (1997)
- ² H. Courtois and B. Pannetier, *J. of Low Temp. Phys.* **118**, 599 (2000)
- ³ K. Inoue and H. Takayanagi, *Phys. Rev. B* **43**, 6214 (1991)
- ⁴ S. H. Tessmer, M. B. Tarlie, D. J. Harlingen, D. L. Maslov and P. M. Goldbart, *Phys. Rev. Lett.* **77**, 924 (1996)
- ⁵ Y. Levi, O. Millo, N. D. Rizzo, D. E. Prober and L. R. Motowidlo, *Appl. Phys. Lett.* **72**, 480 (1998)
- ⁶ M. Vinet, C. Chapelier and J.-F. Lefloch, cond-mat/0004340
- ⁷ H. F. Hess, *Physica B* **169**, 422 (1991)
- ⁸ D. V. Pelekhov, J. B. Becker and G. Nunes, *Appl. Phys. Lett.* **72**, 993 (1998)
- ⁹ C. Bauerle, N. Mori, G. Kurata and H. Fukuyama, *J. of Low Temp. Phys.* **113**, 927 (1998)
- ¹⁰ S. H. Pan, E. W. Hudson and J. C. Davis, *Rev. Sci. Instrum.* **70**, 1459 (1999) ; M. Kugler, Ch. Renner, V. Mikheev, G. Batey and O. Fisher, *ibid* **71**, 1475 (2000)
- ¹¹ The cryostat has been designed at the C.R.T.B.T.-C.N.R.S. by A. Benoit and M. Caussignac. The same is now commercialized by L'Air Liquide.
- ¹² G. Nunes and D. Williams, *J. Vac. Sci. Tech. B* **13**, 1063 (1995)
- ¹³ Ch. Renner, Ph. Niedermann, A. D. Kent, and O. Fisher, *Rev. Sci. Instrum.* **61**, 965 (1990)
- ¹⁴ J. Lindahl, T. Takanen, and L. Montelius, *J. Vac. Sci. Technol. B* **16**, 3077 (1998)
- ¹⁵ R. C. Dynes, V. Narayamurti and J. P. Garno, *Phys. Rev. Lett.* **41**, 1509 (1978)
- ¹⁶ W. Belzig, C. Bruder and G. Schön, *Phys. Rev. B* **54**, 9443 (1994)